AUTOMATED CHAIN FOR AERODYNAMIC COMPUTATIONS MEETING AIRCRAFT TRIMMING REQUIREMENTS

Ludovic Wiart*, David Hue*, Gérald Carrier*
ONERA – The French Aerospace Lab, F-92190 Meudon, France.
ludovic.wiart@onera.fr;david.hue@onera.fr;gerald.carrier@onera.fr

Keywords: *aerodynamics, flight mechanics, aircraft trimming, empennage, aeroelasticity*

Abstract

The present paper focuses on an automated calculation chain developed at ONERA for the generation of aerodynamic polars ensuring trim in the longitudinal axis of the aircraft. This CFD process is carried out with Chimera techniques and through a coupling of the RANS ONERA-elsA solver with a search algorithm calculating adequate trimming surface deflection. The capability of considering flexible wing has also been included in the automated chain, using a simplified structure model. Calculations have been successfully performed with deviations to target pitching moment and lift coefficients smaller than 10^{-4}.

1 Context and Objectives

Nowadays, the successful development of numerical methods for solving the Reynolds averaged Navier-Stokes (RANS) equations and the availability of substantial computational resources give to the Computational Fluid Dynamics (CFD) approach a role of prime importance in the aircraft design process. Data can be generated relative to performance (lift and drag levels), handling quality (aerodynamic moments) or aerodynamic loads applied to the lifting surfaces.

Nevertheless, the current use of CFD consists in the flow calculation for a fixed geometry in given aerodynamic conditions, thus leading to uncontrolled position of the centre of pressure. The centre of pressure of an aircraft is the point where the total sum of a pressure field acts and may be represented by a single force vector with no moment. However, in the frame of a design process, the aircraft maker needs to determine the aerodynamic behaviour in steady, equilibrated flight, i.e. when the centre of pressure and the centre of gravity coincide.

The "classic" approach to this issue is similar for CFD and wind-tunnel measurements. Sweeps are run with different control surface deflection values and the balanced conditions are derived through linear interpolation. For CFD, this implies numerous costly calculations to rebuild a trimmed polar, with possible inaccuracy issues due to interpolation. In wind tunnels, the limiting factor is the impossibility, in most cases, to deflect the control surfaces wind-on. CFD is not subject to such constraints. The proposed approach thus intends to enable the use of control surface deflection in order to trim the aircraft in the course of the aerodynamic calculation.

The present paper presents the automated trimming platform centred on the *elsA* software and the results obtained on test cases representative of modern transport aircraft.

2 Geometries, Meshing Strategies and Flow Solver

The geometry that has been mainly used for this study is the wing-body-horizontal tail NASA Common Research Model (CRM) [1]. This configuration (see Fig. 1) is suitable for investigating trimming issues and numerous associated grids are available thanks to the Committee and participants of the 4th AIAA Drag Prediction Workshop [2][3][4]. A business aircraft geometry in take-off configuration has also been used for validation purpose.

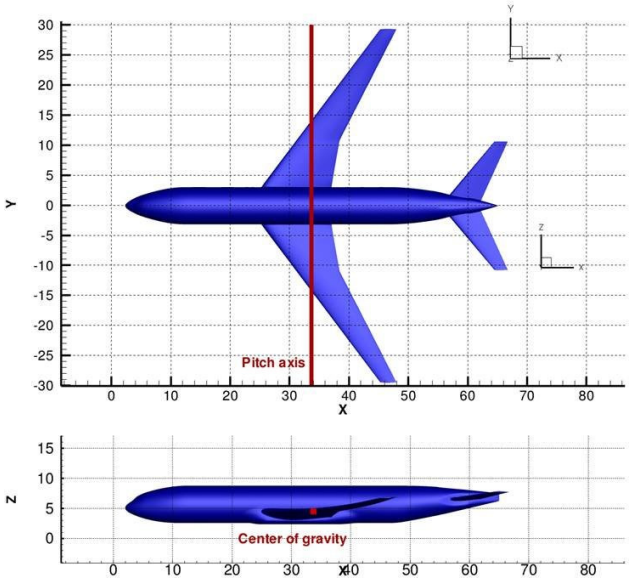

Fig. 1. NASA CRM Geometry

The main objective is, as specified, the generation of trimmed polars. Technically, it is necessary to set up an efficient automated process which determines the deflection of a trimming surface in order to place the centre of pressure location at the centre of gravity for a specified aerodynamic condition (angle of attack or lift). In the frame of this study, only longitudinal trimming has been considered and a single control surface used to meet the balanced condition.

Another objective, of high interest for the aircraft manufacturer, is the ability to evaluate the trim drag of a configuration. The trim drag is here defined as the difference between the tail-off configuration and the trimmed configuration drags at the same lift level. This requirement led us to favour an overset approach, in which the horizontal tail plane (HTP) can be integrated in the wing-body (WB) mesh, and to be easily rotated within the iterative trimming process. The overset techniques available at the time of the study imposed the introduction of a gap between the HTP and its supporting surface to avoid body interpenetration during rotations and to guarantee successful Chimera interpolations between the grids.

In the CRM case, a significant gap was introduced between the fuselage and the HTP root. HTP The resulting overset grid counts 13 million nodes. In the low-speed case, the gap between the vertical tail plane (VTP) and the horizontal stabilizer was reduced to 5 cm for a 1.2 m HTP root chord, due to improved Chimera techniques. The resulting grid counts 27 million nodes.

The RANS computations are performed with the ONERA *elsA* code [5][6][7][8]. This software solves the compressible three-dimensional RANS equations by using a cell-centred finite volume spatial discretization on structured multi-block meshes. Computations are carried out using an uncoupled time stepping scheme for the mean flow and turbulent variables. A backward-Euler time integration scheme is associated with a LUssor scheme for the implicit phase. For the turbulent variables, the Roe numerical scheme is used. Finally, computations have been carried out in fully turbulent mode with the Spalart-Allmaras turbulence model on a SGI ICE 8200 supercomputer.

3 Preliminary Computations

Some preliminary computations were carried out on the CRM configuration at a Mach number of M=0.85, using multi-grid algorithm for convergence acceleration.

At first, the impact of the HTP/fuselage gap was investigated. Calculations were performed both on the generated overset grid and on a 1-to-1 abutting structured multi-block mesh provided by the DPW4 Committee and including the HTP sealed to the fuselage side. The HTP deflection angle δ is set to 0°. The results are presented in Table 1 and as it could be expected, the introduced gap has a significant effect on the aerodynamic coefficients, particularly on lift and pitching moment.

From this comparison, it appears that to accurately account for the HTP effect, the actual intersection geometry should be conserved. Some possible improvements, relying on recent Chimera developments, may allow to overcome this meshing issue and will be discussed later in the paper.

α=0° δ=0°	Baseline grid	HTP overset w/ 50 cm gap
CL fuselage	0.018	0.0215
CL wing	0.168	0.169
CL HTP	-0.033	-0.027
CL total	0.153	0.1635
CD fuselage	83.3	83.2
CD wing	94.8	95.6
CD HTP	12.7	13.6
CD total	190.8	192.4
CM total	0.071	0.036

Table 1. Impact of the HTP/Fuselage Gap

However, in the frame of the study whose outcomes are presented here, emphasis was put on the feasibility and on relative comparisons, therefore the available Chimera approach was considered satisfactory for demonstration purpose.

To obtain a reference database using the "classic" approach, a first set of computations using the Chimera technique has been carried out on the overset grid. Angle of attack (α) sweeps have been run with fixed HTP deflections δ. The sign convention adopted for δ is the same as for α. The results are presented in Fig. 2 and illustrate the influence of the HTP deflection on the pitching moment.

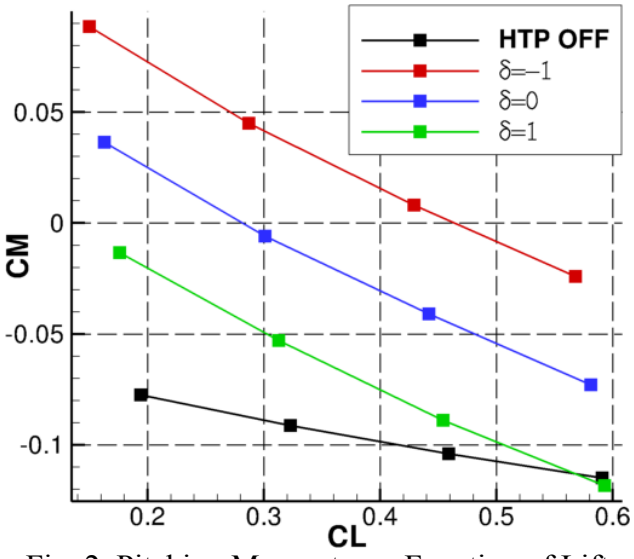

Fig. 2. Pitching Moment as a Function of Lift

With this method and the associated results, it is possible, through interpolation, to evaluate the HTP deflection which trims (i.e. Cm=0 about the centre of gravity) the aircraft over a range of aerodynamic conditions. However, interpolation methods would quickly reach their limits if the interest is on the surface load distribution or on other non-scalar data. The automated chain presented below is aimed at meeting this target with a better accuracy and a reduced number of CFD computations.

4 Trimming Chain Implementation

An automated chain, coupling the *elsA* CFD software to a Newton search algorithm (see Fig. 3.), has been implemented. The basic feature of this chain is to efficiently reach a targeted pitching moment for the specified angle of attack (case 1) or lift coefficient (case 2). In case 1, the HTP deflection angle is the only parameter of the Newton algorithm, whereas in case 2, both the angle of attack of the aircraft and the HTP deflection angle are parameters. Therefore, contrary to the calculations presented in the former paragraph where the HTP was fixed along a polar, this process enables to directly generate a trimmed polar for which, at each computed point, the trimming is insured.

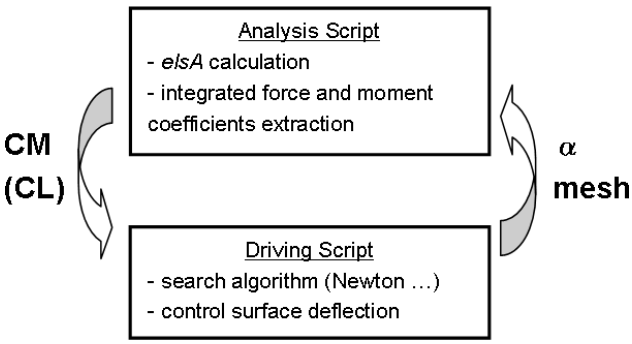

Fig. 3. Trimming Platform

4.1 Single Parameter Case

The Newton algorithm allows to derive the value of δ that will cancel the linear approximation of the CM-CM_{target} function (1). The user has to specify the starting value δ_0, the step Δδ used for the calculation of the CM-CM_{target} function derivative by finite differences as well as the convergence criterion, both for the

mono-dimensional search and the CFD calculation.

$$\delta_1 = \delta_0 - \frac{CM(\delta_0) - CM_{target}}{\frac{dCM}{d\delta}(\delta_0)} \qquad (1)$$

The $\Delta\delta$ step has to be chosen small enough to enable sufficient accuracy, but not too small since it could lead to erroneous detection of the aerodynamic fluxes convergence, thus implying biased gradient evaluation. A value of $\Delta\delta$=0.25° was used in all presented calculations.

CFD computations need the angle of attack and a convergence criterion as inputs. The user can also specify the number of CFD cycles after which the state of convergence should be checked. For the presented test cases, it is checked every 200 cycles, after a first 500 cycles run. Finally, the user can impose any convergence criterion based on the fluxes. A criterion based on the lift has been used here so that the CFD calculation is considered converged for $|CL_i-CL_{i-1}|<\varepsilon_{CFD}$, with CL_i the lift value at one check and CL_{i-1} at the previous one. This simple test is necessary but not sufficient to ensure convergence. A more comprehensive verification should include monotony and bounds violations checks, on more than one aerodynamic coefficient. Of course, reducing the value of ε_{CFD} increases significantly the number of CFD cycles required to satisfy the corresponding convergence level as illustrated in Fig. 4. The search algorithm stops when $|CM-CM_{target}|<\varepsilon_{CM}$. The choice of ε_{CM} value directly impacts the number of calls to the search algorithm.

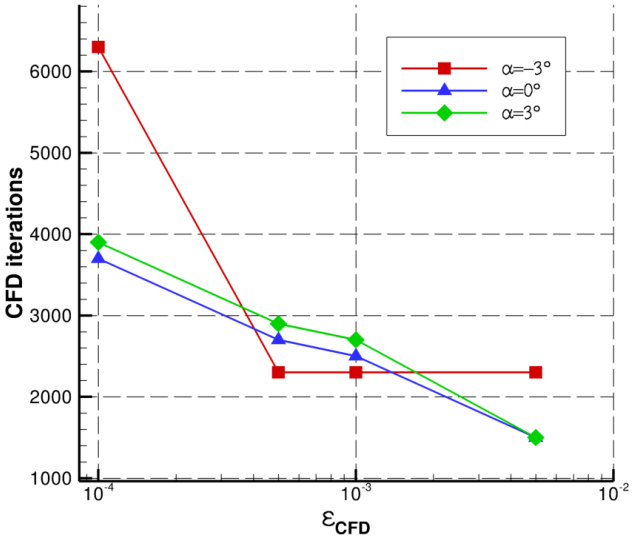

Fig. 4. Influence of Tolerance on Computational Cost for Three Angles of Attack

We chose to set $\varepsilon_{CM}=\varepsilon_{CFD}$ and analyzed the sensibility of the predicted HTP trimming angles and of the aerodynamic coefficients to ε_{CM}. Four different values were tested and the results obtained with the most demanding one ($\varepsilon_{CM}=10^{-4}$) are taken as reference. The deviations (Δ) to the reference HTP deflection, lift and drag values are plotted in Fig. 5. The results obtained by linear interpolation from fixed HTP α-sweeps results are included for comparison purpose. The scatter produced by different ε_{CM} values compared to the reference one seems reasonable, except for ε_{CM}=0.005 which probably is too large for the considered test case. If the agreement of the interpolated data with those obtained with the automated trimming process is rather satisfactory in terms of HTP deflection angle, the aerodynamic coefficients prediction exhibits a greater disparity. It is then up to the user to make a compromise between the desired accuracy and the computational cost in the choice of ε_{CFD} and ε_{CM}. In the rest of the paper, values of $\varepsilon=\varepsilon_{CFD}=\varepsilon_{CM}$=0.001 were considered.

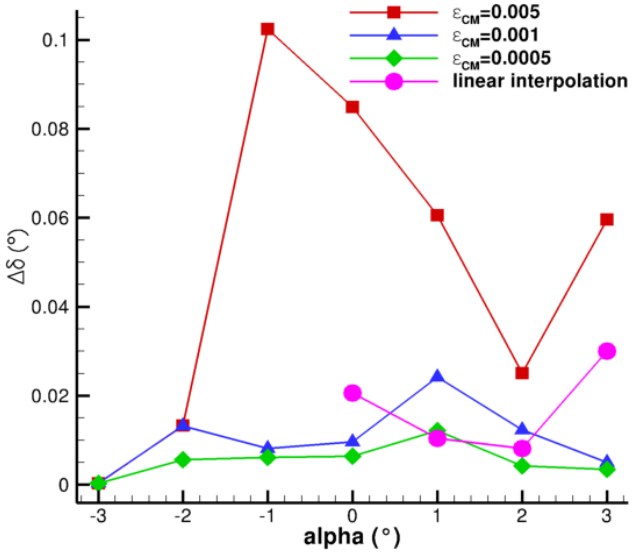

a) Discrepancies in HTP deflection prediction

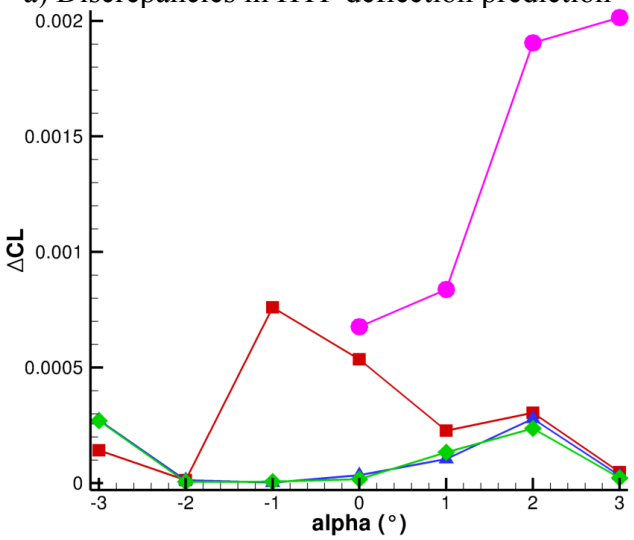

b) Discrepancies in lift level prediction

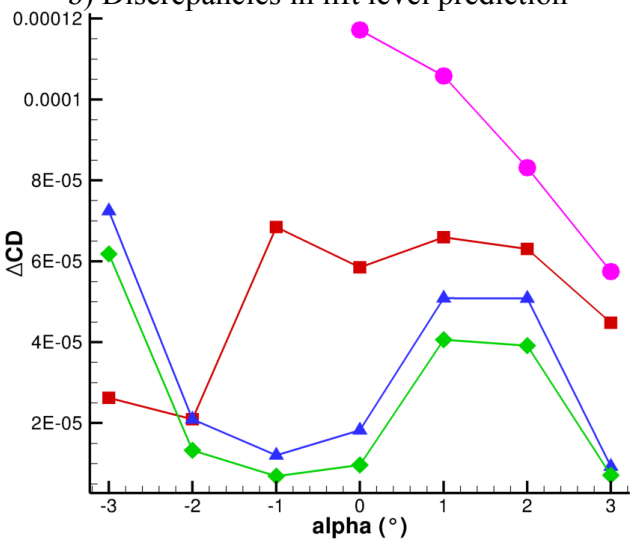

c) Discrepancies in drag level prediction

Fig. 5. Influence of Tolerance Value ε_{CM} on Trimming Accuracy ($\varepsilon_{CM}=10^{-4}$ taken as reference)

4.2 Two-Parameter Case

The trimming platform has been extended to cases for which the lift level is not a result anymore but a constraint. This means that it is necessary to iterate both on the angle of attack and on the HTP deflection angle to satisfy the conditions $|CL-CL_{target}|<\varepsilon$ and $|CM-CM_{target}|<\varepsilon$. The selected algorithm is directly derived from (1) but extended to the two parameters α and δ (2).

$$\begin{bmatrix}\alpha_1\\ \delta_1\end{bmatrix}=\begin{bmatrix}\alpha_0\\ \delta_0\end{bmatrix}-\left[F'(\alpha_0,\delta_0)\right]^{-1}\begin{bmatrix}CL-CL_{target}\\ Cm-Cm_{target}\end{bmatrix} \quad (2)$$

$$with \quad F'(\alpha_0,\delta_0)=\begin{bmatrix}\partial CL/\partial\alpha & \partial CL/\partial\delta\\ \partial Cm/\partial\alpha & \partial Cm/\partial\delta\end{bmatrix}$$

Fig. 6. illustrates the convergence of lift and pitching moment using algorithm (2) with $CL_{target}=0.5$ and $CM_{target}=0$. After 8 iterations of the Newton search algorithm, the $\varepsilon=10^{-3}$ tolerance is achieved and $\varepsilon=10^{-4}$ after 15 iterations.

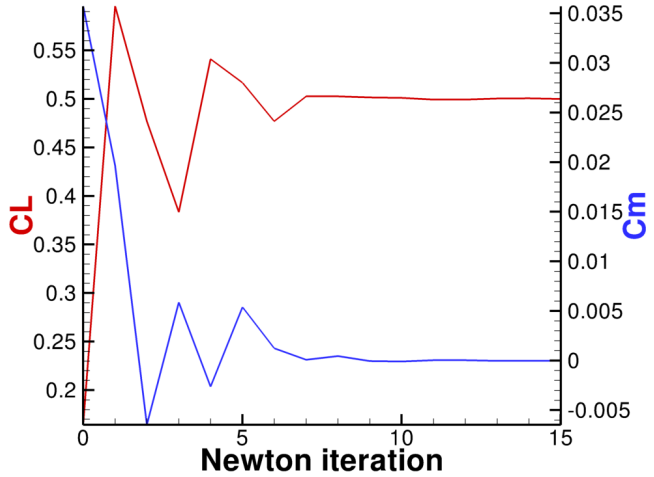

Fig. 6. Newton Search Algorithm Convergence in a Two-Parameter Case ($CM_{target}=0$, $CL_{target}=0.5$)

5 Trimmed Polars

The previous section described the methods implemented in the developed trimming platform, its sensitivity to different parameters and its capabilities. Further analysis of the CRM configuration will now be discussed, including an aeroelastic study, before the investigation of a low speed test case.

5.1 Transonic Cruise Conditions: CRM

Fig. 7 illustrates the capabilities of the trimming platform by opposition to the set of polars obtained with fixed HTP deflection angles (classically used for interpolation purpose).
Fig. 7a shows the gain provided by the automated trimming approach both in terms of computational cost and implementation. As a matter of fact, the "classic" approach would consist in three separate and successive CFD runs, while the proposed approach provides the desired solution in a single run. Besides, greater accuracy is expected in regions where the CM(δ) function exhibits non-linear behaviour.
Fig. 7b illustrates the magnitude of HTP deflection angles required to trim such a configuration around cruise conditions, a 5° deflection range allowing to trim the aircraft in a 6° angle of attack range.
Fig. 7c and
Fig. 7d illustrate the advantages of the proposed approach over a "classic" approach.

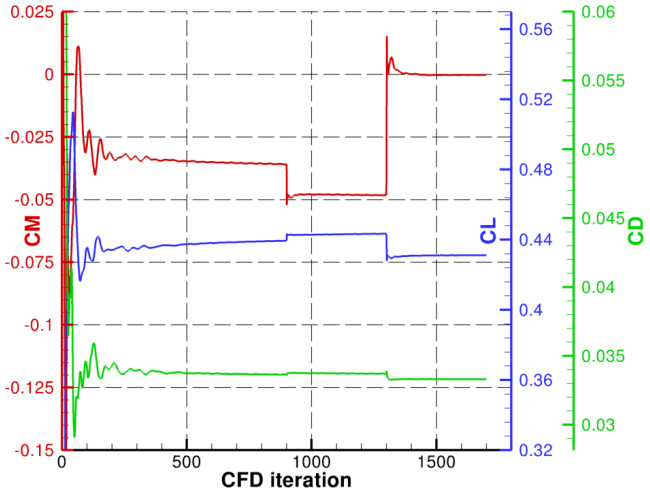

a) Convergence of aerodynamic coefficients during the trimming process (α=2°)

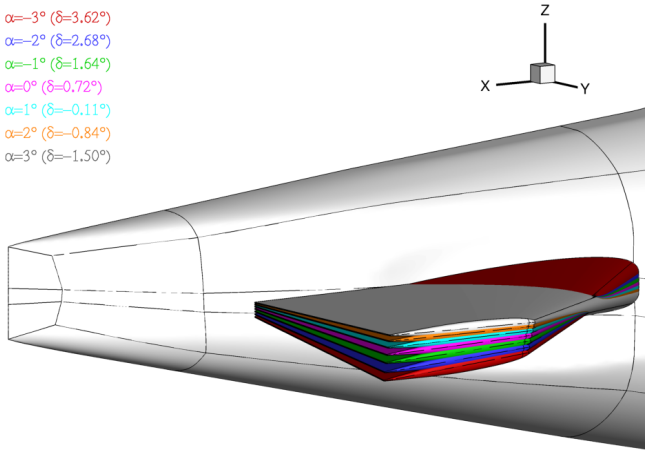

b) HTP deflections in trimmed conditions

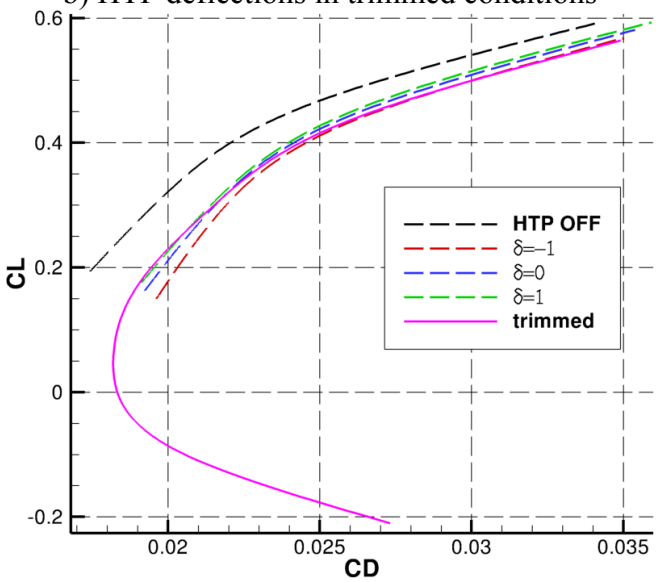

c) Comparison of the automatically trimmed polar with tail-off and fixed HTP calculations

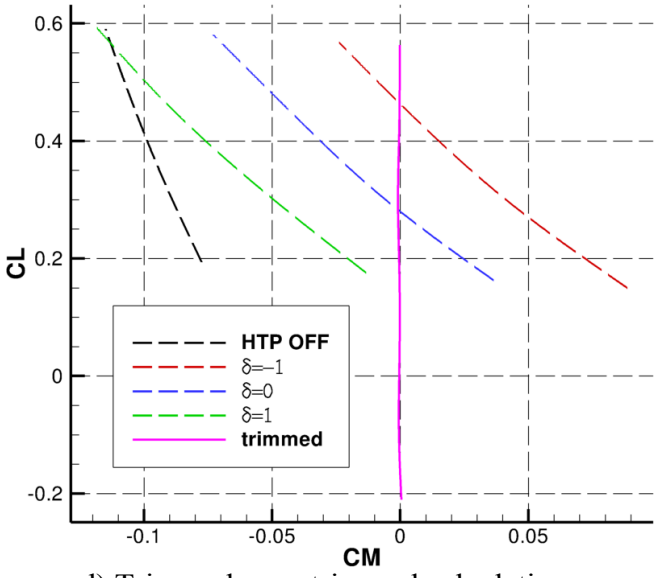

d) Trimmed vs untrimmed calculations

Fig. 7. Application of the Trimming Platform to the NASA CRM Configuration

By comparison of the obtained results with a calculation performed on the tail-off configuration at CL=0.5 too, the trim drag value can be derived (see Table 2). It is worth noticing that to compensate the lift loss induced by the negative tail load, the aircraft has to fly at higher angle of attack. Given the significant magnitude of the trim drag calculated for cruise conditions, representing more than 12% of total drag, the consideration and reduction of this drag component in the design process is of prime importance. It has to be reminded that the trimmed results were obtained on a modified geometry including a significant gap between the HTP and the fuselage.

CL=0.5	Tail-off	Trimmed
α	2.21	2.47
δ	X	-1.19
CM	-0.12	-0.0001
CD (d.c.)	255	291
Trim drag (d.c.)	36	

Table 2. Trim Drag Evaluation at CL=0.5

The trimming platform has been extended to take into account fluid-structure interactions. A simplified beam model [9] of the Common Research Model wing has been coupled to the solver *elsA*, so that the static aeroelastic equilibrium is determined at each *elsA* call. Although this beam model can be calibrated to match experimental deformation data [9], these latter were not available at the time of this study. Therefore, a "generic" structure model was generated to obtain wing bending and twist representative of conventional transport aircraft (see Fig. 8) which is satisfactory to demonstrate the method feasibility.

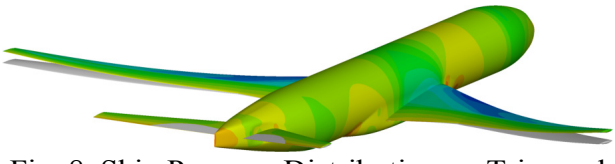

Fig. 8. Skin Pressure Distribution on Trimmed Deformed Shape (α=3°; δ=-1.5°; undeformed shape in gray)

Static aeroelastic calculations were then integrated in the trimming platform. These computations are more expensive than the "rigid" ones, both in terms of CFD iterations (4,900 vs 1,700 at α=2°) to reach the aeroelastic equilibrium and in terms of Newton iterations (2 vs 1 at α=2°). The value jumps observed in Fig. 9 are not due to HTP deflection only as previously, but also to the coupling between *elsA* and the structure model.

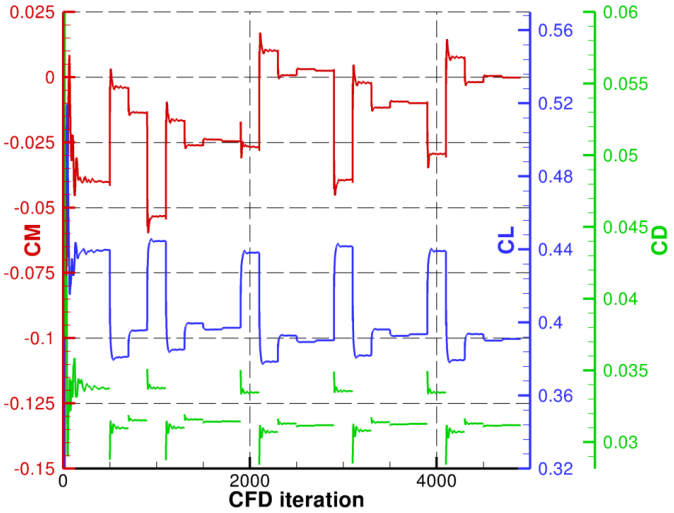

Fig. 9. Aerodynamic Coefficients Convergence during the Trimming Process(α=2°)

Fig. 10 shows the influence of the wing flexibility at fixed angle of attack: the twist of the wing leads to reduced lift and drag. It also impacts the pitching moment magnitude and thus the HTP deflection angle necessary to trim the aircraft, whose magnitude is significantly modified in the aeroelastic case.

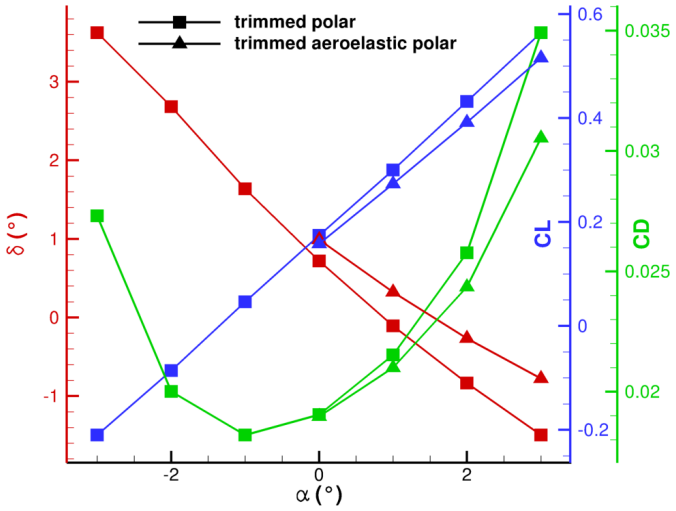

Fig. 10. Influence of Wing Flexibility on Predicted Lift, Drag and HTP Deflection Angle

5.2 Low Speed Conditions: Business Aircraft Configuration

It was important to verify that the trimming platform developed on a transonic test case would be operational for a low speed configuration and flow condition as well.

The selected geometry is a business aircraft in take-off configuration with a T-tail (see Fig. 11). The mesh of the glider is used as background mesh. The flap, vertical tail plane (VTP) and HTP are added through Chimera techniques. As in the CRM case, a gap has been introduced between the VTP and the HTP to allow good interpolations between the body grids.

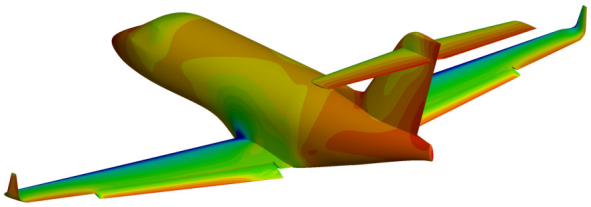

Fig. 11. Skin Pressure Distribution on Trimmed Business Aircraft Configuration (α=9°, δ=-2.24°)

The computations are carried out at a Mach number of M=0.158. Low speed pre-conditioning is used to accelerate the convergence. Fig. 12 illustrates the cost of a trimmed calculation; only 18,000 CFD iterations are necessary while the convergence of a single calculation requires at least 10,000 iterations.

The results of trimming calculations at four different angles of attack are gathered in Fig. 13. It is worth noticing that the dependency between the calculated δ and the corresponding α is not linear for high angles of attack.

Fig. 14 illustrates the HTP effect, which yields a low magnitude negative lift but with a large lever arm from the centre of gravity, in order to compensate the nose-down pitching moment generated by the high-lift wing.

.

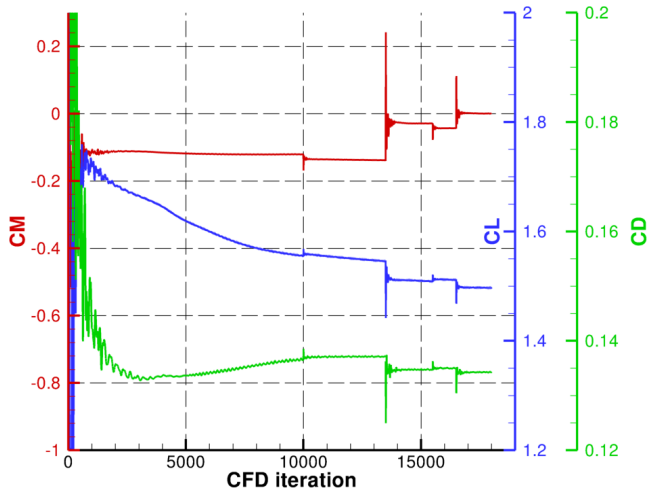

Fig. 12. Convergence of Aerodynamic Coefficients during the Trimming Process (α=9°)

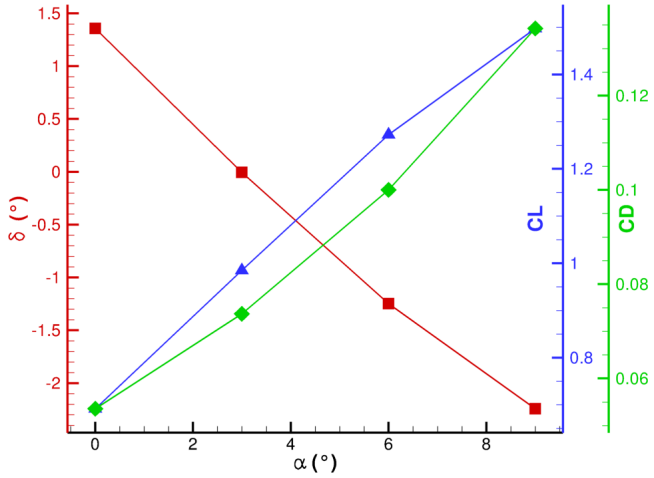

Fig. 13. Results for the Trimmed Aircraft at different Angles of Attack

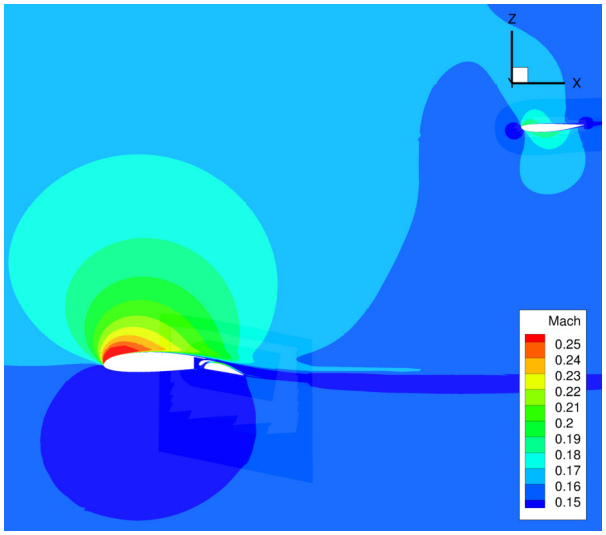

Fig. 14. Mach Number Field (α=9°)

6 Conclusions and Perspectives

This paper focuses on methods for the generation of aerodynamic data for aircraft in trimmed conditions. An automated trimming platform using the *elsA* software has been implemented at the Applied Aerodynamics Department of ONERA. It automatically calculates the horizontal stabilizer deflection angle leading to longitudinal equilibrium about a specified centre of gravity location. It was successfully validated on two configurations representative of modern transport aircraft, at transonic and subsonic speeds. The applicability of the platform to a flexible wing has also been demonstrated.

As it has been mentioned previously, the addition of an horizontal stabilizer on a fuselage or a vertical stabilizer and the management of the bodies intersection during its deflection introduces a meshing issue. Some recent developments in the Chimera techniques [10] make possible the automated generation of collar grids. The HTP mesh could then be extended inside the fuselage or VTP body, the intersection being managed by a collar grid that could be regenerated for each deflection angle. These new capabilities are illustrated in Fig. 15 and could eliminate the need to introduce a gap between the HTP and the fuselage (or VTP).

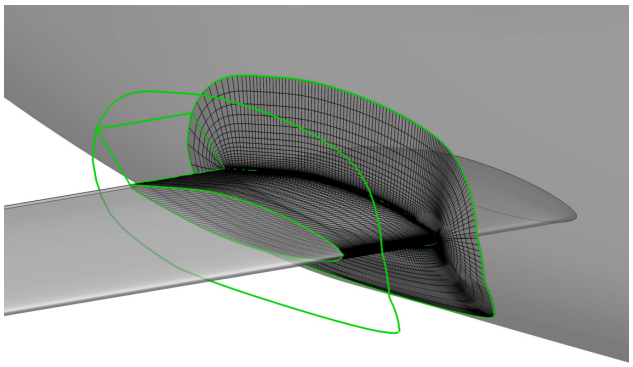

Fig. 15. Example of a Collar-grid Generation at the Junction of Interpenetrating Bodies

Moreover, the approach developed in the frame of this study could be of high interest for optimization purpose. As a matter of fact, an optimization conducted without trimming requirements could reduce the drag for a given angle of attack or CL, but deteriorate the longitudinal stability to the point of being counterproductive once the trim drag is accounted for. If the configurations treated in this paper are rather conventional, it should be mentioned that other aircraft concepts are more demanding in terms of trimming requirements: supersonic aircraft due to the aerodynamic centre shift from subsonic to supersonic flight; canard concepts; blended wing body and box wing designs for instance.

An extension to the simultaneous deflections of several trimming surfaces could also be considered, representing a step further in flight mechanics considerations and possibly trajectory simulations.

Acknowledgments

The authors gratefully acknowledge financial support for this research from the French National Research Agency (ANR) through CARNOT funding.

References

[1] Vassberg J.C, DeHann M.A, Rivers S.M and Wahls R.A. Development of a common research model for applied CFD validation studies. *26th AIAA Applied Aerodynamics Conference*, Honolulu, Hawaii, AIAA Paper 2008-6919, 2008.

[2] Vassberg J.C et al. Summary of the fourth AIAA CFD Drag Prediction Workshop. *28th AIAA Applied Aerodynamics Conference*, Chicago, Illinois, AIAA Paper 2010-4547, 2010.

[3] Hue D, Esquieu S and Gazaix M. Computational drag and moment prediction of the DPW4 configuration using the elsA software. *28th AIAA Applied Aerodynamics Conference*, Chicago, Illinois, AIAA Paper 2010-4547, 2010.

[4] Hue D and Esquieu S. Computational drag prediction of the DPW4 configuration using the far-field approach. *AIAA Journal of Aircraft*, Vol. 48, No. 5, pp 1658-1670, 2011.

[5] Cambier L and Gazaix M. elsA: an efficient object-oriented solution to CFD complexity. *40th AIAA Aerospace Sciences Meeting and Exhibit*, Reno, NV, AIAA Paper 2002-0108, Reno, 2002.

[6] Gazaix M, Jolles A and Lazareff M. The elsA object-oriented computational tool for industrial applications. *23rd congress of ICAS*, Toronto, Canada, 2002.

[7] Cambier L, Gazaix M, Heib S, Plot S, Poinot M, Veuillot J.P, Boussuge J.F and Montagnac M. An

overview of the multi-purpose elsA flow solver. The Onera Journal, *AerospaceLab Journal*, Issue 2, March 2011 (www.aerospacelab-journal.org).

[8] Reneaux J, Beaumier P and Giroudroux-Lavigne P. Advanced aerodynamic applications with the elsA software. The Onera Journal, *AerospaceLab Journal*, Issue 2, March 2011 (www.aerospacelab-journal.org).

[9] Wiart L and Carrier G. Accounting for wing flexibility in the aerodynamic calculation of transport aircraft using equivalent beam model. *13th AIAA/ISSMO Multidisciplinary Analysis Optimization Conference*, Fort Worth, Texas, AIAA Paper 2010-9135, 2010.

[10] http://elsa.onera.fr/Cassiopee/Userguide.html

Copyright Statement